J. Fluid Mech. (2007), *vol.* 576, *pp.* 297–323.
doi:10.1017/S0022112006004435 Printed in the United Kingdom

Overturning in a filling box

N. B. KAYE AND G. R. HUNT

Department of Civil and Environmental Engineering, Imperial College London, Imperial College Road, London, SW7 2AZ, UK

(Received 28 January 2005 and in revised form 30 September 2006)

Overturning in a cylindrical filling box driven by a turbulent plume is examined theoretically and experimentally. We establish the initial penetration depth (h) of the buoyant flow that intrudes vertically up the sidewall as a function of the box radius (R) and height (H). Dimensional arguments reduce the problem to finding $\eta = h/H$ as a function of the aspect ratio $\Phi = R/H$. The flow is modelled in two parts, the radial outflow from the plume along the base of the box and the flow up the sidewall. The outflow is modelled as a forced radial gravity current with constant buoyancy flux while the sidewall flow is modelled as a line fountain. Two regimes were found: first, when the plume outflow is adjusting toward a pure gravity current on impact with the vertical wall and the rise height is given by $\eta \sim \Phi^{-1/3}$; secondly, when the outflow is fully developed on, or before, impact and the rise height is given by $\eta \sim$ Const. Experimental results show good agreement with these scalings and allow the constants of proportionality to be established.

1. Introduction

The filling box model was first introduced by Baines & Turner (1969), who examined the time-dependent stratification established by a single turbulent plume in a closed vertical cylinder of radius R and height H with an initially uniform environment. The plume from a localized buoyancy source at the base ($z = 0$) rises to the top of the box ($z = H$) and spreads out radially, forming a buoyant layer. The continuous supply of increasingly buoyant fluid causes the layer to deepen and the density front to approach the plume source. Baines & Turner (1969) developed a model for the movement of the density front and the stratification produced in the box once all the environment had been recycled through the plume. They assumed that the initial outflow from the plume formed a horizontal layer of zero thickness at time $t = 0$ and that turbulence in this deepening layer rapidly decayed as it became part of the environment. However, in their experiments, they found that whilst this assumption was reasonable for aspect ratios $H/R \ll 1$,† for narrower boxes (larger H/R) the outflow from the plume overturned after colliding with the vertical sidewall and mixed with the ambient. The dynamics of this mixing were not included in their model. Baines & Turner (1969) balanced the destabilizing momentum force ($\sim \pi w^2 b^2|_{z=H}$) associated with the plume of vertical velocity w and width b impinging on the box ceiling with the stabilizing buoyancy force ($\sim \pi R^2 b g'|_{z=H}$), where g' is the buoyancy of the plume, associated with the layer. They thereby demonstrated that the degree of overturning, hereafter referred to as the stability of the flow, is a function of a purely geometric parameter,

† Baines & Turner (1969) define the box aspect ratio as H/R. However, we scale all lengths on the box height H and, therefore, define the aspect ratio of the box as $\Phi = R/H$.

namely, the box aspect ratio H/R. They also demonstrated that the flow is stable, that is with negligible overturning, for $H/R < 1$. This conclusion is supported by their experimental results. Note that this geometric result is only valid for a pure fully developed turbulent plume from a point source for which $b \sim H$. For a non-pure source (either forced or lazy) that has fully adjusted on reaching $z = H$, a virtual origin correction is needed.

A full analytic solution for the flow in the box and exterior to the plume was developed by Manins (1979). Manins (1979) also found that the solution was stable for $H/R < 1$. While Baines & Turner (1969) assumed an initial layer of infinitesimal depth, Manins (1979) found the initial layer occupied a quarter of the depth of the box. This depth is significantly larger than we found in our experiments (§ 5). Wong, Griffiths & Hughes (2001) examined the flow structure in the ambient fluid outside the plume experimentally. They again found that the initial layer was approximately a quarter of the box depth and that the ambient flow was separated into various bands of inflow and outflow relative to the plume. Worster & Huppert (1983) developed a series solution for the transient buoyancy profiles.

The flow in filling boxes with aspect ratios greater than unity was studied by Barnett (1991). Barnett found that for sufficiently large aspect ratios ($H/R \gtrsim 4$) the downflow in the ambient that balances the upflow in the plume plays a critical role, and for $H/R \gtrsim 5.8$ the plume no longer reaches the top of the cylinder but is destroyed by shear-induced turbulence between the rising plume and the down-flowing ambient. Hunt, Cooper & Linden (2001) examined the stratification established in wide boxes (low H/R) as well as the effects of a forced plume in a filling box and modified the model of Baines & Turner (1969) to account for the plumes source momentum flux. Additionally, they considered simultaneous momentum-flux and buoyancy-flux inputs from separate sources.

The filling box model was extended by Linden, Lane-Serff & Smeed (1990), who examined a filling box that was connected, via openings in the top and base, to an external quiescent ambient. They used this model to examine buoyancy-driven ventilation flows in buildings. In this application the plume rises to the top of the box and spreads out as in the filling box of Baines & Turner (1969). However, as the buoyant layer deepens, the hydrostatic pressure difference between the internal and external environments drives a flow through the openings. Therefore, instead of the buoyant layer filling the entire space, the buoyancy and volume fluxes that flow through the box due to the pressure difference balance the fluxes into the buoyant layer from the plume leading to a steady two-layer stratification and displacement flow.

In practice, displacement flow has the advantage of leading pollutants, or stale air, away from the lower occupied regions of a room into a buoyant layer near the ceiling, while drawing fresh exterior air into the occupied regions (Hunt & Kaye 2006). It is, therefore, of interest from a design viewpoint to establish the parameter range over which this flow is stable. Overturning of the upper layer during the initial transients may result in stale and polluted air being reintroduced into the occupied areas of the room.

Another context in which the filling box model has been applied is confined fire plumes. Of concern is, for example, the rate at which a room will fill with smoke produced by a small fire in the centre of the floor. Again, there is considerable interest in the overturning of the plume outflow at the sidewall. Alpert (1975) models the outflow from a fire plume impinging on a horizontal ceiling as a radial jet that increases in depth with radius. This result is used by Cooper (1988) to examine

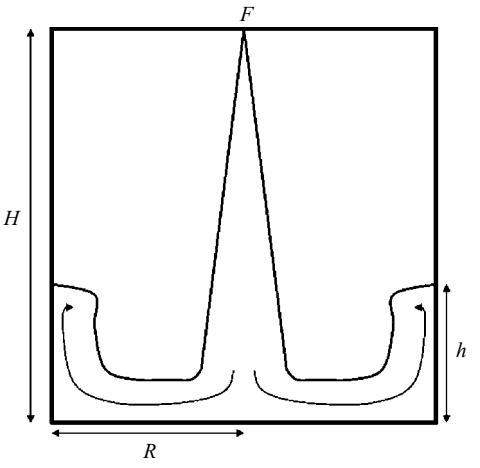

FIGURE 1. Schematic showing a confined descending plume of buoyancy flux F colliding with a horizontal surface, spreading out radially and then rising up the sidewalls and overturning.

the ceiling jet when it is turned down by sidewalls. Cooper (1988) examines aspect ratios of $H/R > 1$ and finds that the initial maximum vertical penetration depth (h) is a constant fraction of the room height ($h/H \approx 0.8$). Cooper (1988) claims that Baines & Turner (1969) would have found the same result if they had used a larger Reynolds number plume source in their experiments. Jaluria & Kapoor (1992) examine experimentally the wall flow driven by a buoyant ceiling jet. They produce penetration depth correlations in terms of the outflowing buoyant jet Richardson number. Kapoor & Jaluria (1996) extend the range of Richardson numbers considered earlier and also present heat transfer correlations for the flow.

In all this work, a complete model is not presented for the penetration depth of the overturning flow along the wall as a function of the box aspect ratio (figure 1). In this paper we consider a negatively buoyant, pure, localized, axisymmetric Boussinesq plume of source buoyancy flux F centrally located at the top of a closed cylinder of radius R and height H. For wide cylinders ($H/R < 1$) the plume will descend to the base of the box and spread radially outwards forming a buoyant layer that deepens over time. This flow is well described by the filling box model of Baines & Turner (1969) and Worster & Huppert (1983). For narrower cylinders, the initial outflow from the plume rises vertically up the side of the container and overturns (or slumps back; see § 5) as it collapses back under gravity. The greater the aspect ratio, the greater the depth of penetration h of this overturning. In the limit of a very narrow container the plume will be influenced by upflow in the environment before it reaches the base (Barnett 1991; Huppert *et al.* 1986).

A goal of this paper is to quantify the extent of the overturning during the initial transient in the unstable regime intermediate to the 'filling box' (Baines & Turner 1969) and 'blocked' regimes (Barnett 1991), that is, for $1 < H/R \lesssim 4$. We develop a two-part model of the flow. Part one considers the outflow from the plume whose development close to the impingement region we model as a forced radial gravity current with a constant buoyancy flux. Part two treats the flow up the sidewall as a line wall fountain with source conditions given by the outflow model.

In § 2 we review the various models proposed for the outflow produced by a plume impinging on a horizontal surface. We draw an analogy between classifying radial

gravity currents and classifying plumes in terms of their respective source conditions. We demonstrate that the adjustment region for the radial flow, namely, the radial distance over which the flow adjusts to a constant-Froude-number gravity current, may be regarded as similar to the characteristic vertical length scales of either forced plumes (Morton 1959) or lazy plumes (Hunt & Kaye 2005), which themselves adjust to a pure plume in the far field. The details of the adjustment process and the radial extent over which it occurs are not well understood, although modelling this adjustment is central to the present study. Knowledge of the process of transition from vertical plume flow to horizontal gravity current flow is key to understanding a number of flows of practical interest. For example, the near-field mixing of a buoyant sewage plume impinging on the surface of the sea will be controlled by the dynamics of this adjustment region. We show in § 2 that, for a pure plume impinging on a horizontal boundary, the flow in the adjustment region is a forced radial gravity current regardless of the source–boundary separation. From this result we develop equations describing the volume and momentum fluxes in the current as a function of radius and outflow source conditions. This model is compared to our experimental results. In § 3 we model the vertical wall flow as a turbulent line fountain. We review existing work on point source and line source fountains and re-scale these results to give the rise height up the sidewall as a function of the plume outflow parameters of § 2. Section 4 brings these two models together and makes predictions for the penetration depth as a function of the box aspect ratio. Experiments to verify the outflow front position and penetration depth predictions are presented in § 5 and conclusions are drawn in § 6.

2. Outflow from a plume impinging on a horizontal surface

We consider the collision of an axisymmetric constant-buoyancy-flux turbulent plume from a point source with a horizontal boundary in a quiescent uniform environment. (In general, the environment in a filling box will be stratified and this stratification will affect the plume outflow. However, we are only concerned with the initial transient when the box is 'empty'. There is then no stratification to consider.) A schematic of the flow and the nomenclature adopted is given in figure 2. The radial coordinate with origin on the plume's vertical axis is denoted by r and the depth of the outflow by $\Delta(r)$. In practice these flows are relatively common, for example, a fire plume or a thermal plume from a heat source in a room impinging on a ceiling (in this case a solid boundary), or a buoyant waste-water plume reaching the surface of the sea into which it is released. We restrict our attention to solid boundaries and to situations where the density difference between the plume and the surroundings is small compared with the density of the surroundings so that the Boussinesq approximation is valid.

On impinging with the boundary, the flow from the plume will spread horizontally outwards and, in the far field, develop into a constant-Froude-number radial gravity current. Near the point of impact, however, there is an adjustment region, of horizontal extent r_a, over which the flow develops into a pure gravity current – here we use 'pure' to refer to a current with a constant Froude number. We assume that in the impingement zone (shaded region of figure 2) there is no mixing with the ambient.†

† This assumption would lead to the plume volume and momentum fluxes and the plume radius at the point of impingement being calculated at $H - \Delta_0$ rather than at H (2.10). This would result in a correction of order $(1 - \Delta_0/H)^{5/3}$ to the volume flux, $(1 - \Delta_0/H)^{4/3}$ to the momentum flux

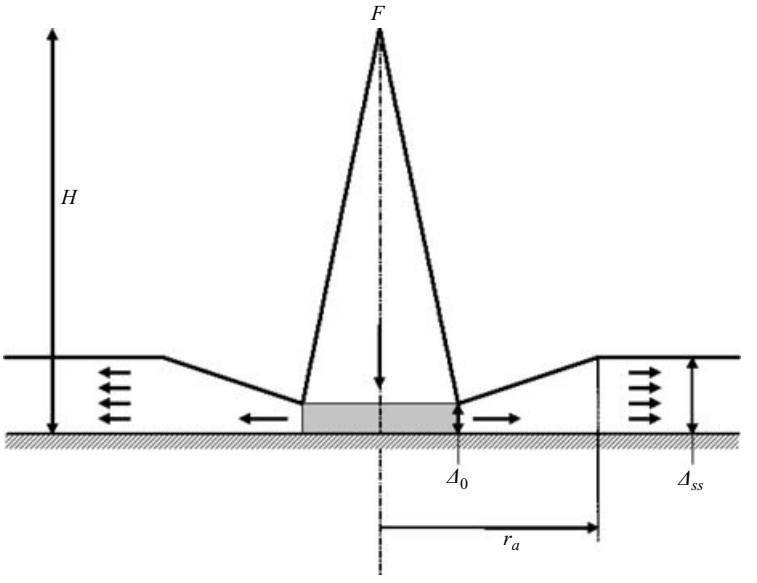

FIGURE 2. Schematic of the outflow from a dense pure plume impinging on a horizontal boundary showing the nomenclature adopted. The impingement zone is shown by the shaded area below the plume.

The only entrainment into the flow occurs in the plume above the impingement zone, and in the outflow at radial distances greater than the plume radius at the point of impingement. This assumption is consistent with the assumption made by Lee & Jirka (1981) and implies that the volume flow rate in the plume at the boundary will be equal to the volume flow rate in the outflow at the outflow source.

We begin by stating a key result relating to the spread of constant buoyancy flux radial gravity currents before considering the near-source adjustment region. We then present a model (§ 2.1) for the bulk properties of the outflow and compare our predictions to experimental measurements (§ 5.1) of the outflow front movement.

Chen & List (1977) balance the buoyancy force ($\rho g' \Delta^2$) and inertial force ($\rho r^2 \Delta / t^2$) to establish a relationship ($r = c_i F^{1/4} t^{3/4}$) for the position of the front of a gravity current outflow with time (t) for the inertial regime. Following on from this work, Britter (1979) solves the governing shallow-water equations and obtains the same time scalings. Experimental results from Britter (1979) suggest $c_i = 0.84$, hence

$$r = 0.84 F^{1/4} t^{3/4}. \tag{2.1}$$

2.1. *Source conditions and length scales*

For a constant buoyancy flux radial gravity current the main parameters are the current depth ($[\Delta] = L$), radial distance ($[r] = L$) and buoyancy flux ($[F] = L^4 T^{-3}$). The other parameters of note are the volume flux ($[Q] = L^3 T^{-1}$) and momentum flux ($[M] = L^4 T^{-2}$) which can be expressed in terms of Δ, r and F. Assuming the fully developed flow (i.e. for sufficiently large r) has a constant depth, as observed by Britter (1979), and denoting the horizontal velocity by v (independent of depth),

and $(1 - \Delta_0/H)$ to the plume radius. However, as the plume is assumed pure, the balance of the fluxes and the plume Froude number will be unchanged and, therefore, this $O(10^{-1})$ correction to the fluxes is neglected in our analysis that follows.

we can use dimensional analysis to develop scalings for the volume flux ($2\pi r v \Delta$), momentum flux ($2\pi r v^2 \Delta$) and velocity of the current

$$Q = C_1 \Delta F^{1/3} r^{2/3}, \; M = C_2 \Delta F^{2/3} r^{1/3}, \tag{2.2}$$

and

$$v = \frac{\mathrm{d}r}{\mathrm{d}t} \sim F^{1/3} r^{-1/3}. \tag{2.3}$$

It is also possible to obtain the latter result by differentiating (2.1) to give

$$v = \frac{\mathrm{d}r}{\mathrm{d}t} = 0.59 F^{1/3} r^{-1/3}, \tag{2.4}$$

which can be used to estimate the values of the constants $C_1 = 3.7$ and $C_2 = 2.2$ needed to complete (2.2). The flow's buoyancy is therefore given by $g' = F/Q \sim F^{2/3} r^{-2/3} \Delta^{-1}$. From this, (2.4) and (2.2) we can define a Froude number for the flow as

$$Fr = \frac{v}{\sqrt{g' \Delta}} \sim \frac{F^{1/3} r^{-1/3}}{\sqrt{(F^{2/3} r^{-2/3} \Delta^{-1}) \Delta}} = \text{Const.} \tag{2.5}$$

If the 'source' conditions which characterize the supply of fluid to the current do not result in this Froude number at the current source, as will in general be the case, there will be an adjustment region (in the near field) before the flow becomes a 'pure' constant buoyancy flux radial gravity current (in the far field). In the 'pure' constant buoyancy flux flow the gravity current is still entraining fluid ($Q \sim r^{2/3}$). Therefore, the outflow buoyancy decreases with increasing radial distance from the centre.

These equations give straightforward estimates of the volume and momentum fluxes at a given radial distance, but for chosen values of the fluxes Q and M they can be inverted to provide an estimate of the radial distance a current of buoyancy flux F would need to travel in order to obtain those flux values. It is in this sense that we define two radial length scales, namely, the volume flux length scale (r_Q) and the momentum length scale (r_M)

$$r_Q = 3.7^{-3/2} \Delta_0^{-3/2} Q_0^{3/2} F^{-1/2}, \tag{2.6}$$

$$r_M = 2.2^{-3} \Delta_0^{-3} M_0^3 F^{-2}, \tag{2.7}$$

where the subscript '0' indicates the source value for the current. Note that the plume and the current source buoyancy fluxes are identical ($F = F_0 = \text{constant}$) as the environment is unstratified; we assume that there are no transfers of buoyancy between the fluid and the boundary. Drawing an analogy with the theory for forced (Morton 1959) and lazy (Hunt & Kaye 2005) plumes, the current can be regarded as 'forced' if $r_M > r_Q$, 'lazy' if $r_M < r_Q$ and 'pure' if $r_M = r_Q$. In line with plume theory, the forced current has an excess of source momentum flux and the lazy current a deficit compared with a constant Froude number (pure) current of identical buoyancy flux. We can also define a ratio of these length scales analogous to that for plumes,

$$\Gamma_0 = \frac{r_Q}{r_M} = 1.5 \frac{Q_0^{3/2} \Delta_0^{3/2} F^{3/2}}{M_0^3}, \tag{2.8}$$

and, thus, the flow in the adjustment region can be regarded as 'forced' for $\Gamma_0 < 1$, 'pure' for $\Gamma_0 = 1$ or 'lazy' for $\Gamma_0 > 1$. As discussed previously, the corrections to the volume and momentum fluxes and plume radius due to the presence of the mixing zone had powers of 5/3, 4/3 and 1, respectively. Substituting these corrections into (2.8) we see that all the corrections cancel, indicating that our use of the plume flux

values at the lower boundary makes no difference to the controlling parameter of the outflow Γ_0.

Note that this discussion differs from the predictions of some analytical models, such as Britter (1979), that suggest that the similarity solution is independent of all but the source buoyancy flux. However, this latter result is based on the assumption that there are no imposed length scales at the source. In general this is not the case, and the similarity solution will only be valid at the source if the imposed source length scales r_Q and r_M are equal.

For a highly forced current one would expect a development region for small r ($<r_M$) that behaved as a radial wall jet. For a smooth boundary this is a constant momentum flux flow with a linear increase in current depth with radius as observed by, for example, Lee & Jirka (1981) and Lawrence & MacLatchy (2001).

The 'source' conditions for the current are those supplied by the pure plume. Assuming top-hat profiles in the plume, following Morton, Taylor & Turner (1956), the radius (b_p), volume flux (Q_p) and momentum flux (M_p) at the boundary can be expressed as

$$b_p = \frac{6\alpha_t H}{5} \approx 0.15H, \tag{2.9}$$

$$Q_p = \pi \left(\frac{5F}{8\pi\alpha_t}\right)^{1/3} \left(\frac{6\alpha_t H}{5}\right)^{5/3} = 0.16F^{1/3}H^{5/3}, \tag{2.10}$$

$$M_p = \pi \left(\frac{5F}{8\pi\alpha_t}\right)^{2/3} \left(\frac{6\alpha_t H}{5}\right)^{4/3} = 0.35F^{2/3}H^{4/3}, \tag{2.11}$$

where we have taken $\alpha_t = 0.09\sqrt{2}$ (see Hunt & Kaye 2001) as the plume entrainment coefficient appropriate for top-hat profiles. We use (2.9) as the radius at which the current begins. Continuity requires (2.10) to be the source volume flux of the current. As the plume impinges on the horizontal surface the vertical momentum flux will be reduced to zero. There will also be energy losses as the flow changes direction at the solid boundary.

As there is only one length scale for the problem of a pure plume impinging on a horizontal surface, namely, the distance (H) from the plume point source to the boundary, all other length scales for the flow will scale linearly on this height. Therefore, the plume radius and, consequently, the outflow source radius r_0 as well as the outflow source thickness Δ_0 will scale on H. Conservation of volume can then be applied to the control volume shown (shaded) in figure 2 to give

$$Q_p = \pi r_0^2 w = 2\pi r_0 \Delta_0 v. \tag{2.12}$$

Since the length scales r_0 and Δ_0 both scale on H, (2.12) implies that $w \sim v$. We can therefore write an expression for the radial outflow's 'momentum flux'

$$M_0 = 2\pi r_0 \Delta_0 v^2 \sim \pi r_0^2 w^2 \sim M_p. \tag{2.13}$$

Hence

$$M_0 = \gamma M_p \tag{2.14}$$

where γ is a constant. Note that the total radial momentum flux of the flow integrated around the circumference is required to be zero by conservation of momentum flux as there is no radial component of momentum in the pure plume. However, the 'momentum flux' quantity given by (2.13) can still be evaluated and used to characterize the level of shear expected at the source. It can then be used to calculate

the values of r_M and Γ_0 to give a balance between the destabilizing shear of the flow and the stabilizing buoyancy force. In general, the above scaling argument implies that

$$2\pi r_0 \Delta_0 v^n \sim \pi r_0^2 w^n. \tag{2.15}$$

So, for example, one would expect that the kinetic energy flux ($n = 3$) of the outflow would be a constant fraction of the kinetic energy flux of the plume at the point of impingement.

One could argue that the parameter γ would be a function of various non-dimensional groups such as the plume Froude number at the point of impingement. It could also be influenced by background stratification. However, we are considering only point source pure fully developed turbulent plumes that have a constant Froude number at all heights, and an unstratified ambient. A similarity argument can then be made that γ will be constant for all such pure plume impingement flows. Furthermore, if γ were not a constant, as assumed herein, it would not have been possible to collapse all our experimental data for the outflow front movement as shown in figure 10.

The boundary conditions on the radial outflow are now

$$r_0 = 0.15H, \quad Q_0 = 0.16F^{1/3}H^{5/3} \tag{2.16}$$

and

$$M_0 = \gamma M_p = 0.35\gamma F^{2/3}H^{4/3}. \tag{2.17}$$

Therefore, the source depth of the current is given by

$$\Delta_0 = \frac{Q_0^2}{2\pi r_0 M_0} = \frac{0.068}{\gamma}H, \tag{2.18}$$

which implies that the initial outflow depth increases as the energy loss due to the change in flow direction increases (that is, γ decreases).

Evaluating the length scales defined in (2.6) and (2.7) using (2.16)–(2.18) leads to

$$r_Q = 0.41\gamma^{3/2}H \quad \text{and} \quad r_M = 7.1\gamma^6 H, \tag{2.19}$$

and hence

$$\Gamma_0 = 0.58\gamma^{-9/2}. \tag{2.20}$$

We note the particularly sensitive dependence of r_M and Γ_0 on γ, and that (2.20) indicates that the flow is forced ($\Gamma_0 < 1$) near the point of impingement if $\gamma > 0.53$. Lee & Jirka (1981) suggest that the energy loss due to plume impingement is analogous to losses due to a 90° bend in a pipe and cite an energy loss of 20%. Combining (2.14) and (2.15) with this energy loss value gives a value of $\gamma \approx 0.9$. Therefore, we expect $\Gamma_0 < 1$ (from (2.20)) and, thus, the outflow to be forced.

We therefore assume that the outflow behaves as a turbulent radial momentum jet near the point of impingement with no loss in momentum flux as the flow spreads along the (smooth) boundary. This turbulent flow will entrain ambient fluid and is expected to increase linearly in depth with radius (Bakke 1957). Turbulent entrainment will change the balance of fluxes in the current and will increase the local value of $\Gamma(r)$ until it reaches the pure gravity current balance of $\Gamma(r) = 1$. The flow will then be described by (2.1). For a constant momentum flux wall jet we have

$$\Delta = \frac{\mathrm{d}\Delta}{\mathrm{d}r}(r - r_0) + \Delta_0 \quad \text{and} \quad M = M_0 = 0.35\gamma F^{2/3}H^{4/3}, \tag{2.21}$$

where $\mathrm{d}\Delta/\mathrm{d}r$ and γ are our unknown constants, and r_0 and Δ_0 are given by (2.16) and (2.18), respectively. Carrying these unknowns through we can express the velocity

$v(r)$ and volume flux $Q(r)$ as

$$v = \sqrt{\frac{M_0}{2\pi r \Delta}} = \frac{\gamma^{1/2}\sqrt{0.35}F^{1/3}H^{2/3}}{\sqrt{2\pi r \Delta}} \tag{2.22}$$

and

$$Q = \sqrt{2\pi r \Delta}\gamma^{1/2}\sqrt{0.35}F^{1/3}H^{2/3}. \tag{2.23}$$

To leading order in r, the outflow depth is given by $\Delta \approx (\mathrm{d}\Delta/\mathrm{d}r)r$. This approximation is valid provided $(\mathrm{d}\Delta/\mathrm{d}r)r$ is greater than $(\mathrm{d}\Delta/\mathrm{d}r)r_0 - \Delta_0$, which is the difference between two terms of order 10^{-1}. Hence, using (2.22) we estimate the movement of the front with time in the adjustment region as

$$\frac{\mathrm{d}r}{\mathrm{d}t} \approx \sqrt{\frac{0.35}{2\pi}}\sqrt{\frac{\gamma}{\mathrm{d}\Delta/\mathrm{d}r}}\frac{F^{1/3}H^{2/3}}{r}. \tag{2.24}$$

This is valid for $r \gg r_0$, which is reasonable provided $r_a \gg r_0$. Integrating (2.24) gives

$$r \approx 0.69\left(\frac{\gamma}{\mathrm{d}\Delta/\mathrm{d}r}\right)^{1/4}F^{1/6}H^{1/3}t^{1/2} \tag{2.25}$$

to leading order in r.

We now introduce length and time scales based on the vertical separation H and the plume buoyancy flux F. Dimensionless time τ and radial coordinate ϕ, respectively, are defined as

$$\tau = \frac{t}{H^{4/3}F^{-1/3}} \quad \text{and} \quad \phi = \frac{r}{H}. \tag{2.26}$$

In the near-field (forced) adjustment region the non-dimensional front position, from (2.25), is

$$\phi = 0.69\left(\frac{\gamma}{\mathrm{d}\Delta/\mathrm{d}r}\right)^{1/4}\tau^{1/2}, \tag{2.27}$$

and for the far-field pure gravity current flow described by Britter (1979), (2.1), we get

$$\phi = 0.84\tau^{3/4}. \tag{2.28}$$

In order to establish the value of the constant in (2.27) and the radial extent of the forced adjustment region we turn to laboratory experiments (see § 5).

There is considerable debate about the exact nature of the near-source outflow. Our experiments indicate (figures 12 and 13) the presence of a gravity current like head on the flow. This head has been characterized as a ring vortex in other contexts (Patterson *et al.* 2006). It could, therefore, be argued that the behaviour of the ring vortex dominates the front movement of the flow. The ring vortex from a lock release gravity current has recently been studied by Patterson *et al.* (2006), who found that the ring vortex at the front of the gravity current had three distinct phases. The first two phases were characterized by two different constant velocity regions. This constant velocity behaviour is not observed in our experiments (see figure 9).

Clearly the current that flows behind the head of the outflow influences the front movement. This behaviour has similarities with the starting cap on a point source plume. Turner (1962) showed that, although the starting cap on a plume looks like a thermal, the trailing plume flow constrains the radial growth of the cap and controls its velocity. By analogy, the head of the outflow examined herein is controlled by the flow behind, and the ring vortex behaviour described by Patterson *et al.* (2006)

is not observed. Furthermore, given that the outflow is 'forced', that is, momentum-dominated, it can be regarded as super-critical and therefore controlled at the source, rather than by the fluid buoyancy. Therefore, in the near-source region, the flow will behave as a wall jet.

In the far field, the source conditions should have no influence on the flow development and the flow should behave as a constant buoyancy flux radial gravity current as described by Britter (1979). The adjustment from the forced flow to the fully developed buoyancy-driven flow can be attained either through an internal hydraulic jump, or via mixing and energy dissipation in the jet-like near-source region (Wilkinson & Wood 1971). For the case of a plume impinging on a horizontal surface, experimental observations of (Lawrence & MacLatchy 2001, abstract) 'provide no compelling reason to postulate the existence of an internal hydraulic jump'. Finally, we note that the front movement predictions of our model accurately describe our experimental results given in § 5 supporting the wall jet (near field) and pure radial gravity current (far field) modelling approach we have adopted.

3. Overturning

We now turn our attention to what happens after the outflow collides with the sidewall of the cylindrical box. We assume that the plume source is centred in the box top so that the radial outflow is symmetric and will collide with the sidewall at the same instant around the circumference. We also assume that the radius of the cylinder is large compared with the depth of the outflow so that, having been turned upwards by the sidewall, the dense flow can be treated as a turbulent line wall fountain. In this section we review the pertinent literature on fountains, focusing on predictions of their rise height. We then re-scale these existing results in order to fit with the scalings used in our description of the outflow. In § 4 we combine the outflow (§ 2) and fountain (§ 3) models to predict the rise height up the wall as a function of the box aspect ratio.

Previous work on gravity currents colliding with a vertical wall focused on one-dimensional lock release gravity currents (see Simpson 1982, p. 175). In this case the fluid rises to a height of approximately twice the initial layer depth. However, the different geometry (axisymmetric as opposed to one-dimensional) and different source conditions (constant buoyancy flux as opposed to constant buoyancy) means that this work is not applicable to our problem. Instead we turn to the literature on turbulent fountains.

Turner (1966) used dimensional arguments to show that the rise height (z_m) of a free axisymmetric fountain is a linear function of the jet length (L_j) of the fountain source $z_m \sim L_j \sim M_f^{3/4} F_f^{-1/2} \sim Q_f {r_f}^{-3/2} {g'_f}^{-1/2}$, where the subscript '$f$' denotes the value at the fountain source; Q_f is the volume flux, r_f the radius, g'_f the buoyancy, M_f the momentum flux and F_f the buoyancy flux. Turner (1966) also provides considerable experimental evidence to support this scaling relationship. Following on from this, Baines, Turner & Campbell (1990) present data on axisymmetric fountains that suggest the rise height scaled on the source radius is a linear function of the source Froude number, i.e. $z_m/r_f = 2.46 Fr_f$ where

$$Fr_f = \frac{U_f}{\sqrt{r_f g'_f}} = \frac{Q_f}{\pi {r_f}^{5/2} {g'_f}^{1/2}}$$

and U_f denotes the vertical velocity at the fountain source. This is the dimensionless form of the jet length scaling.

In a paper on line-source fountains, Goldman & Jaluria (1986) present correlations based on hot gas experiments that relate the rise height to the Grashof number (Gr) and the Reynolds number (Re) of the source defined therein as

$$Gr = \frac{g'_f D_f^3}{\nu^2} \quad \text{and} \quad Re = \frac{U_f D_f}{\nu}, \tag{3.1}$$

where $D_f (= 2r_f)$ is the width of the fountain source and ν is the kinematic viscosity. They present results for both free and wall line fountains,

$$\frac{z_{m.free}}{D_f} = 3.959 \left(\frac{Gr}{Re^2}\right)^{-0.440} \quad \text{and} \quad \frac{z_{m.wall}}{D_f} = 4.424 \left(\frac{Gr}{Re^2}\right)^{-0.389}. \tag{3.2}$$

The quantity Gr/Re^2 is equal to the reciprocal of Fr_f squared,

$$\frac{Gr}{Re^2} = \frac{g'_f D_f}{U_f} = \frac{Q_0^3 F_0}{M_0^3} = \frac{1}{Fr_f^2}, \tag{3.3}$$

meaning that (3.2) can be re-written in terms of the Froude number as

$$\frac{z_{m.free}}{D_f} = 3.959 Fr_f^{0.88} \quad \text{and} \quad \frac{z_{m.wall}}{D_f} = 4.424 Fr_f^{0.78}. \tag{3.4}$$

This suggests that the rise height is slightly less than linear in Fr_f, which is similar to previously published work for axisymmetric fountains.

We now discuss what one might expect to be the differences between a free and wall fountain, and how these differences will affect the fountain rise height. The presence of the wall will tend to cause a frictional drag on the fountain, reducing its vertical momentum flux and, thereby, its rise height. However, for large Reynolds numbers, this effect will be minimal. The wall will also reduce the entrainment as the fountain will only be drawing in ambient fluid from one side. This will tend to allow the fountain to rise to a greater height as entrainment acts to reduce the rise height ($z_m \sim \alpha^{-1/2}$ for highly forced fountains; see Kaye & Hunt 2006). These two wall effects act against each other. Based on this observation, along with the correlations of Goldman & Jaluria (1986) (see (3.4)), it appears that there are only minor differences between the rise heights of wall and free line fountains.

We therefore model the rise height of our side-wall flow as a turbulent fountain with rise height given by

$$\frac{z_m}{D_f} = C Fr_{fl}, \tag{3.5}$$

where the parameter C (taken to be a constant) is a function of the entrainment coefficient (α_{fl}) appropriate for a line fountain. In terms of the source parameter Γ_{fl}, analogous to the outflow source parameter in (2.8), we get

$$\frac{z_m}{D_f} \sim \Gamma_{fl}^{-2/3}, \tag{3.6}$$

where

$$\Gamma_{fl} = \frac{1}{2\alpha_{fl}} \frac{Q_f^3 F_f}{M_f^3}. \tag{3.7}$$

We do not establish the value of these constants in this work, but rather use the rise height scaling in our model development and then verify the qualitative behaviour predicted.

4. Penetration depth model

We now return to the original problem of predicting the overturning of a plume in a cylindrical box (see figure 1). We have established a description of the outflow (2.27) and (2.28) and will model the flow up the sidewall as a turbulent line wall fountain (3.6). We now couple these two models to produce a final expression for the rise height up the wall $\eta = h/H$ as a function of the aspect ratio $\Phi = R/H$. We assume that the aspect ratio of the box and the Reynolds number of the plume are such that viscous forces are negligible (see § 4.3 for more details on these limitations).

Based on the models of § 2 and § 3 we note that the problem can be broken down into two domains: first, where the aspect ratio of the box is large enough ($\Phi > 0.66$) that the outflow is a fully developed pure gravity current on reaching the sidewall (2.28) and, secondly, where the box is sufficiently tall ($\Phi < 0.66$) that the outflow behaves as a buoyant wall jet when it hits the sidewall. This transition value of $\Phi = 0.66$ is based on our experimental results (§ 5).

4.1. *Shorter cylinders* ($\Phi > 0.66$)

We begin by examining cylinders where the aspect ratio is sufficiently large (short boxes) that the outflow is a fully developed pure radial gravity current as it reaches the sidewall.

4.1.1. *Turning region*

In order to couple the two flow descriptions above we need to examine the corner flow where the outflow from the plume is turned upwards and becomes a fountain. This is not too dissimilar to the plume impinging on the base of the box, and similar assumptions will be made. Following the same arguments as in § 4, we assume that the buoyancy and volume fluxes are conserved and that the momentum flux quantity is reduced by a factor γ. We also assume that the thickness of the outflow is small compared to the radius of the box and that, therefore, the wall can be treated as linear and of length $2\pi R$. A schematic of this region is shown in figure 3.

From (2.2) we can write the volume flux and a quantity with dimensions of momentum flux at $r = R$ as

$$Q(r = R) \approx 3.7\Delta_{ss} F^{1/3} R^{2/3} \quad \text{and} \quad M(r = R) \approx 2.2\Delta_{ss} F^{2/3} R^{1/3}. \tag{4.1}$$

We assume that this flow turns upwards at the corner and that a turbulent line fountain forms with source fluxes given by (4.1). For a line fountain, fluxes are expressed per unit length so from (4.1) the source fluxes become

$$Q_f \approx \frac{3.7\Delta_{ss} F^{1/3} R^{2/3}}{2\pi R}, \quad F_f = \frac{F}{2\pi R} \quad \text{and} \quad M_f = \gamma M_R \approx \frac{2.2\gamma\Delta_{ss} F^{2/3} R^{1/3}}{2\pi R}. \tag{4.2}$$

Again we assume that γ is a constant and that, as the flow is being turned through 90°, the value will be similar to that used previously. The actual value is not important as we only make qualitative predictions about how the rise height scales with the box aspect ratio. We can now solve for the source width D_f of the fountain which is given by

$$D_f = \frac{Q_f^2}{M_f} = \frac{\Delta_{ss}}{\gamma}. \tag{4.3}$$

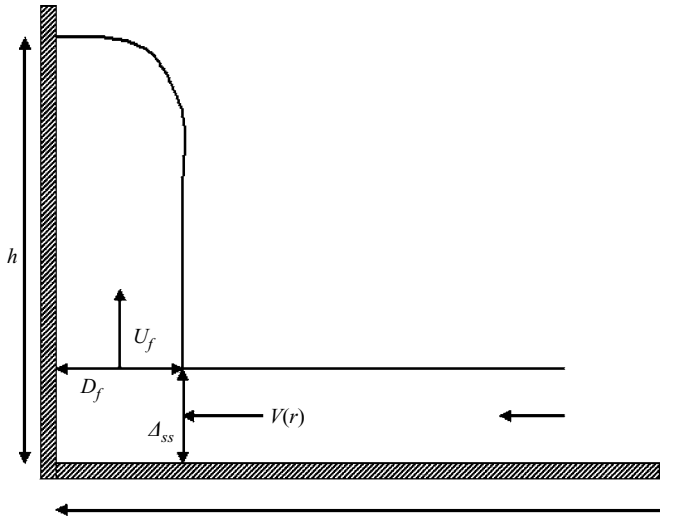

FIGURE 3. Schematic showing a fully developed pure radial outflow from the plume colliding with the box sidewall and turning upwards.

Based on (4.2), (3.7) reduces to

$$\Gamma_{fl} = \frac{1}{2\alpha_{fl}} \left(\frac{3.7}{2.2}\right)^3 \frac{1}{2\pi\gamma^3} = \text{Const}, \tag{4.4}$$

that is, the balance of fluxes at the fountain source is independent of the height or radius of the box. The source length scale (D_f) is given by

$$D_f = \Delta_{ss}/(2\alpha_{fl}\gamma). \tag{4.5}$$

Based on (4.5) and that on dimensional grounds Δ_{ss} scales on the plume height H (see figure 7 for experimental verification), we get

$$D_f \sim H. \tag{4.6}$$

4.1.2. *Rise height*

We now turn to the question of how high up the sidewall the fountain will rise. As the scaled rise height ζ_m ($=z_m/D_f$) is a function of Γ_{fl} only (3.6) and Γ_{fl} is a constant (4.4), we find that the rise height is

$$\zeta_m = \frac{z_m}{D_f} \sim \text{Const}. \tag{4.7}$$

The greatest height the fountain attains is therefore

$$z_m = \zeta_m \times D_f \sim H. \tag{4.8}$$

Although there is significant uncertainty regarding the value of the rise height, it is clear that in the fully developed pure radial gravity current regime the rise height up the sidewall is a function of the box height only and, therefore, not a function of the aspect ratio.

4.2. *Taller cylinders* ($\Phi < 0.66$)

We now turn our attention to boxes that are sufficiently narrow ($R < r_a$) that the outflow collides with the sidewall while in the adjustment region.

4.2.1. *Turning region*

The volume and momentum fluxes as functions of r are known from (2.23) and (2.21); hence we can calculate the fluxes per unit length at $r = R$ as

$$Q_f = \frac{\sqrt{0.35 \times 2\pi R \Delta(r=R)\gamma}\, F^{1/3} H^{2/3}}{2\pi R}, \quad F_f = \frac{F}{2\pi R} \tag{4.9}$$

and

$$M_f = \gamma M(r=R) = \frac{0.35\gamma^2 F^{2/3} H^{4/3}}{2\pi R}. \tag{4.10}$$

This leads to a first-order scaling for Γ_{fl} of

$$\Gamma_{fl} \sim \left(\frac{R}{H}\right)^2. \tag{4.11}$$

We note that this is the same controlling parameter identified by Baines & Turner (1969) expressed there as $I/B = 9\alpha_p/(10(H/R)^2)$.

Assuming, as we did in § 2, that the depth grows linearly with radius for $r_0 < r < r_a$ we have $\Delta \sim R$ at $r = R$. As the outflow turns upwards at the corner we can again calculate the fountain width at the source, D_f, to get

$$D_f = \frac{Q_f^2}{M_f} = \frac{\Delta(r=R)}{\gamma} \sim R. \tag{4.12}$$

4.2.2. *Rise height*

The scaling relationship between the box geometry and fountain source conditions are given by (4.11) and (4.12). Combining these with (3.6) we establish the rise height up the sidewall as

$$z_m = \zeta_m \times D_f \sim \Gamma_{fl}^{-2/3} \times D_f/2\alpha_{fl} \sim \left(\frac{H}{R}\right)^{4/3} \times R \sim H\left(\frac{R}{H}\right)^{-1/3}. \tag{4.13}$$

This implies that as the cylinder gets relatively taller and thinner, that is, R/H decreases, the rise height up the sidewall h/H increases, as observed by Baines & Turner (1969).

4.3. *Full non-dimensional model and limitations*

We have now produced estimates for the rise height z_m of the plume outflow up the sidewall of a cylindrical box for small ($\Phi < 0.66$) and large ($\Phi > 0.66$) aspect ratios $\Phi = R/H$. This rise height is taken to be the maximum initial penetration depth of the flow, that is, $z_m = h$. We now scale these results on the box height and re-state the limits on the applicability of each equation.

Dividing both (4.8) and (4.13) by H, we get the final scaling relationships between the dimensionless rise height $\eta = h/H$ and the box aspect ratio $\Phi = R/H$:

$$\left.\begin{array}{lll} \eta \sim \Phi^{-1/3} & \text{for} & \Phi < 0.66, \\ \eta \sim \Phi^{0} & \text{for} & \Phi \geqslant 0.66. \end{array}\right\} \tag{4.14}$$

We now discuss the practical limitations of our model. The main areas we discuss are viscous forces, the effect of the sidewall on the growth of the plume and scalings for the source velocity at the point of impingement and at the sidewall.

We assume that the plume is fully turbulent at the source. Therefore, the Reynolds number will increase as $Re \sim z^{2/3}$ and viscous forces in the plume can be ignored. In

the outflow, however, viscous forces will become increasingly significant with distance from the plume axis. The distance at which viscosity will play a role was quantified by Britter (1979), who showed that viscous forces will become significant for times greater than $0.4 \times t_*$, where t_* is defined as

$$t_* = Q_0(\nu F)^{-1/2}. \tag{4.15}$$

Substituting (4.15) and (2.10) into (2.1) we obtain the radial distance from the plume axis at which viscous forces become significant:

$$r_* \approx 0.1 H Re^{3/8} \tag{4.16}$$

where

$$Re = \frac{F^{1/3} H^{2/3}}{\nu}. \tag{4.17}$$

This means that for boxes with aspect ratios

$$\Phi > \Phi_* = 0.1 Re^{3/8} \tag{4.18}$$

viscous forces cannot reasonably be ignored, and (4.14) will not apply.

The second possible source of error in our model is the influence of the box sidewall on the development of the descending plume. If the sidewall restricts the plume's development the assumed outflow source conditions will not apply. As mentioned in § 1, this problem was examined by Barnett (1991), who found that for aspect ratios $\Phi \lesssim 0.25$ the movement of the environment surrounding the plume significantly affected the plume dynamics and for $\Phi < 0.17$ the plume would break down. Therefore our model will be restricted to aspect ratios greater than

$$\Phi_{\min} = 0.25. \tag{4.19}$$

Finally, there is significant uncertainty about the value of the parameter γ (2.14) when the plume impinges with the box base and when the outflow hits the sidewall. Based on the experimental results for the outflow presented in § 2 we expect the value to be close to one, and the estimate of Lawrence & MacLatchy (2001) of $\gamma \approx 0.9$ therefore appears to be reasonable. However, uncertainty there, as well as error in using first-order estimates for the radial growth rate of the outflow in the adjustment region means that, without experimental data, we are unable to put meaningful constants in front of the scalings of (4.14). To overcome these problems, and to verify the validity of the scaling relationships developed, a series of laboratory experiments were performed (§ 5) to measure various outflow parameters and the extent of plume overturning in a cylindrical filling box.

5. Experiments

We performed two sets of experiments. The first set examined the plume impingement and resulting outflow, while the second series measured the overturning height for a range of cylinder aspect ratios.

In both sets of experiments the plume was created by supplying a salt solution (NaCl) from a nozzle (designed to produce turbulent flow at the nozzle exit) at constant volume flux. The volume flux was kept steady by the use of a constant-head gravity feed tank. The flow rate was measured using an inline rotameter flow rate meter and was controlled by a needle valve.

Two visualization techniques were used during the course of these experiments. For the overturning experiments and those to measure the adjustment radius, the plume

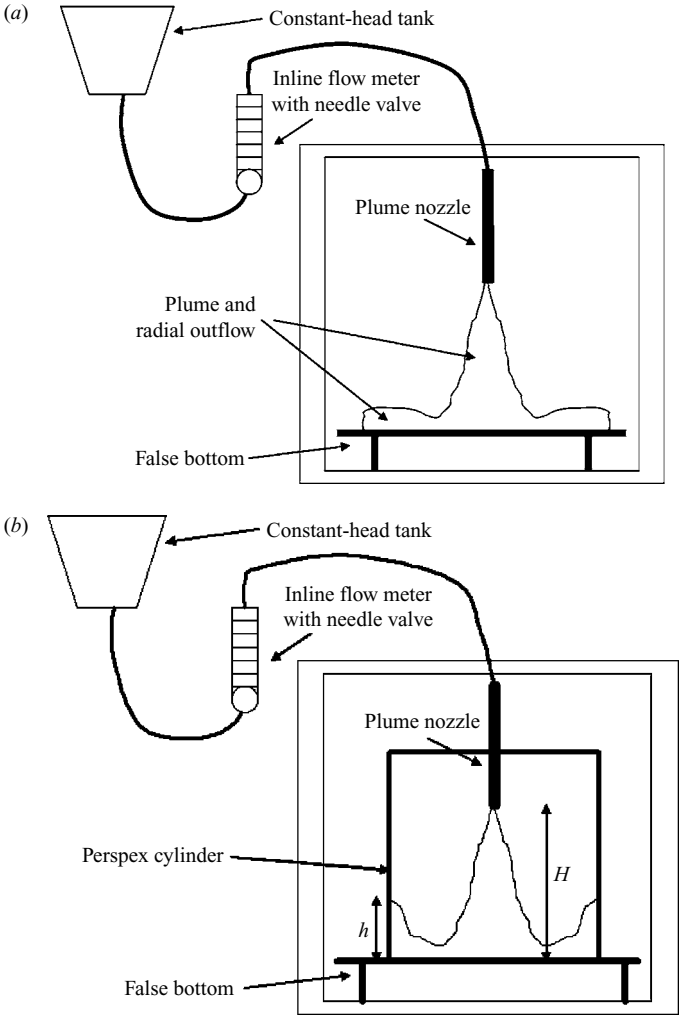

FIGURE 4. Schematic of the experimental setup for (*a*) tracking the front movement and depth of the plume outflow, and (*b*) measuring the overturning height h in the cylindrical box.

fluid was dyed with Sodium Fluorescein. The experiment was then lit using a thin light sheet in the plane of the axis of symmetry and normal to the camera direction of view. This light-induced fluorescence (LIF) technique enabled visualization along a particular radius of the axisymmetric flow, thereby allowing the details of the flow structure to be observed. The experiments concerning the plume outflow front position were visualized using a dye-attenuation technique in which food colouring is added to the plume fluid and the apparatus diffusively back-lit.

The plume outflow experiments were performed in a glass visualization tank (of 1.25 m square base and depth 1.5 m) filled with fresh water. The tank was fitted with a false bottom to aid visualization. The buoyancy flux F and source–boundary separation H were varied for a range of experiments. The source–boundary separation was taken to be the distance from the source to the false bottom plus the distance from the source to the plume virtual origin z_v (see Hunt & Kaye 2001). A schematic of this experimental setup is shown in figure 4(*a*).

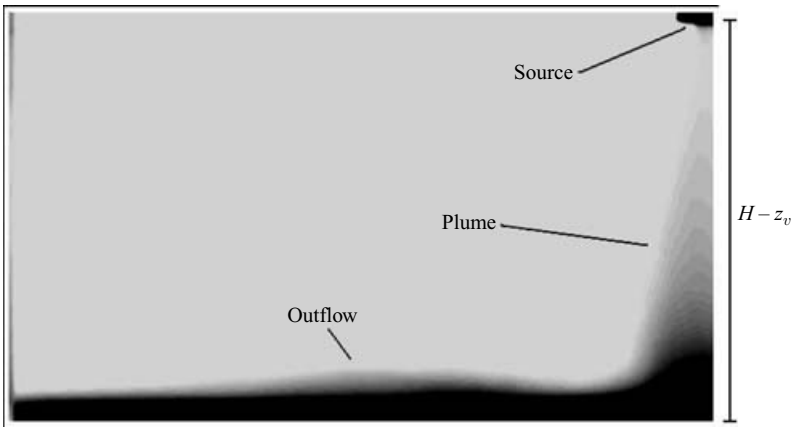

FIGURE 5. A time-averaged image of the outflow showing the radial growth in depth near the outflow source and adjustment to a constant depth gravity current. The right-hand boundary of the image is the plume centreline. The outflow is the horizontal dark-grey region and flows from right to left.

The overturning experiments were performed in a clear Perspex cylindrical tank of radius 22.5 cm and maximum water depth 70 cm. The aspect ratio was set by the height of the plume virtual source above the base of the tank. All experiments described herein were filmed using a CCD digital camera (JAI CV-M4+CL) and the captured images were processed using the DigiFlow software (Dalziel 1993). The digital videos were reviewed to measure the maximum initial rise height h up the sidewall. A schematic of this experimental setup is shown in figure 4(*b*).

5.1. *Plume outflow experiments*

Three separate series of experiments were performed: firstly, a series of LIF experiments measured the adjustment radius of the outflow; secondly, a series of back-lit experiments measured the outflow thickness; finally, another series of back-lit experiments were performed to track the outflow front movement with time. In each set of experiments the plume descended through the ambient fluid and impinged on a horizontal false bottom in the visualization tank. The false bottom was of sufficient width to allow the outflowing current to adjust to a steady depth Δ_{ss} (figure 2) for the range of source–boundary separations (H) considered.

5.1.1. *Jet-like adjustment region*

The first measurement reported here is the dependence of the adjustment radius (r_a) (figure 2) on the source–boundary separation (H). For these experiments the LIF technique was used with the light projected up from below the tank. Once the outflow was fully established, a time-averaged image of the flow was taken (see figure 5 for a typical image averaged over 15 s). We observed that the outflow depth increased with r near the point of impingement, reached a peak and then decreased to an approximately constant value as r increased further. The depth of the outflow was measured based on a cut-off light intensity and was read by eye from the time-averaged images. We took the adjustment radius r_a to be the radial distance at which the outflow depth was a maximum. Beyond this radius the flow no longer behaved as a radial jet, which is characterized by increasing depth with radius. The radial distance to the point of peak depth was measured for 10 experiments over the range $5.5 \leqslant H \leqslant 18.2$ cm. A plot of r_a against H is shown in figure 6 and indicates an

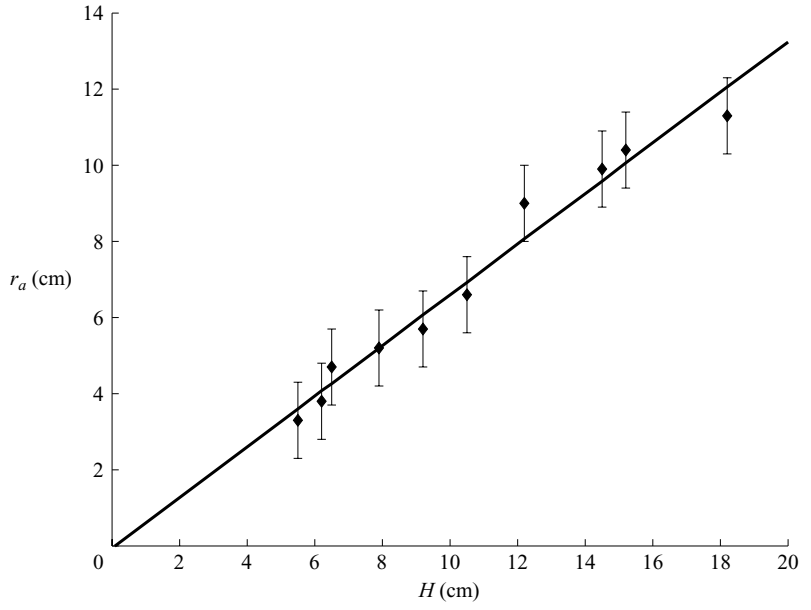

FIGURE 6. Radius r_a at which the outflow attained a maximum depth as a function of the source–boundary separation H. The line is the fit $r_a = 0.66H$.

approximately linear increase in r_a with H. The line plotted is a best fit to the data forced through the origin and is given by

$$r_a = 0.66H. \tag{5.1}$$

We note that the far-field steady-state flow depth Δ_{ss} is less than the peak depth Δ_a at $r = r_a$; see figure 5. The maximum depth was typically around $\Delta_a \approx 0.2H$.

5.1.2. *Outflow depth*

The depth of the fully developed outflow gravity current was measured using the dye attenuation technique (Hacker, Linden & Dalziel (1996)). Measurements of layer depth (Δ_{ss}) against plume-boundary separation (H) for a series of 15 experiments are shown in figure 7. The data follow a linear trend indicating that the steady-state layer depth scales on the plume height as would be expected on dimensional grounds. The line plotted is $\Delta_{ss} = 0.12H$ and is a linear best fit forced through the origin. This gives a dimensionless layer depth of $\delta_{ss} = 0.12$, or approximately $H/8$, for the steady flow at distances greater than the adjustment radius. Again the thickness was measured by eye using a cut-off light intensity.

There is some disagreement about the steady depth of the outflow Δ_{ss} from a plume impinging on the base of a box. Manins (1979) and Wong *et al.* (2001) observed the outflow depth to be approximately $H/4$, whereas our experimental observations indicated $\Delta_{ss} \approx H/8$ (figure 7). We believe that this discrepancy is due to a difference in the definition of the outflow depth and how it is measured. Wong *et al.* (2001) measured depth by tracking a vertical line of dye in the ambient fluid as it was deflected by the outflow and observed that the lowermost quarter of the line was deflected in the direction of the outflow. In our experiments the plume fluid was dyed and the depth of the dyed layer measured. As the goal of this paper is to determine the penetration depth of the buoyant fluid originally from the plume, rather than the

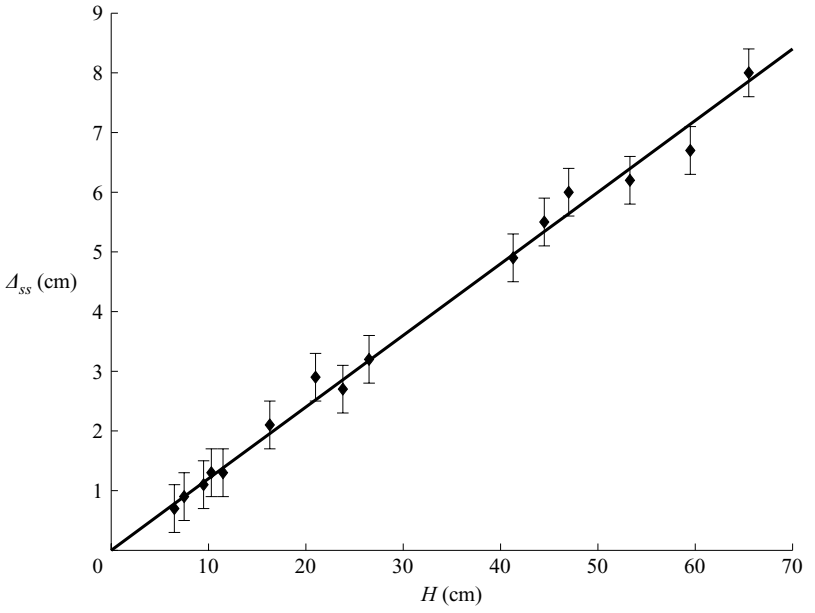

FIGURE 7. Steady depth Δ_{ss} of the outflow downstream of the adjustment region against the source–boundary separation H. The line plotted ($\Delta_{ss} = 0.12H$) is a linear fit to the data forced through the origin.

Experiment	H (cm)	F (cm^4 s^{-3})	Symbol
A	47.5	255	+
B	50.5	255	×
C	21.5	255	*
D	32.3	182	⋆
E	7.1	122	○

TABLE 1. Experimental parameters for the five profiles presented in figure 9.

induced motion in the ambient, we will continue to use our measure of the outflow depth.

5.1.3. *Front movement*

Using the same setup, a series of experiments was run to measure the front position of the outflow as a function of time. A series of images from a typical experiment is shown in figure 8.

A series of five initial experiments (A to E; see table 1) were performed in which the buoyancy flux and source–boundary separation were varied and the front movement tracked over time. The plume was activated and the front movement was videoed. After each experiment the video was reviewed and measurements of the front position against time were recorded. The time was measured to within 0.25 s and the radial distance to within 2 mm. The time origin was taken as the moment the plume made contact with the horizontal boundary. Measurements of front movement against time are plotted in figure 9. Sixty-five further experiments were run in which the location of the front at $t = 10$ s and the time taken for the front to reach $r = 20$ cm were

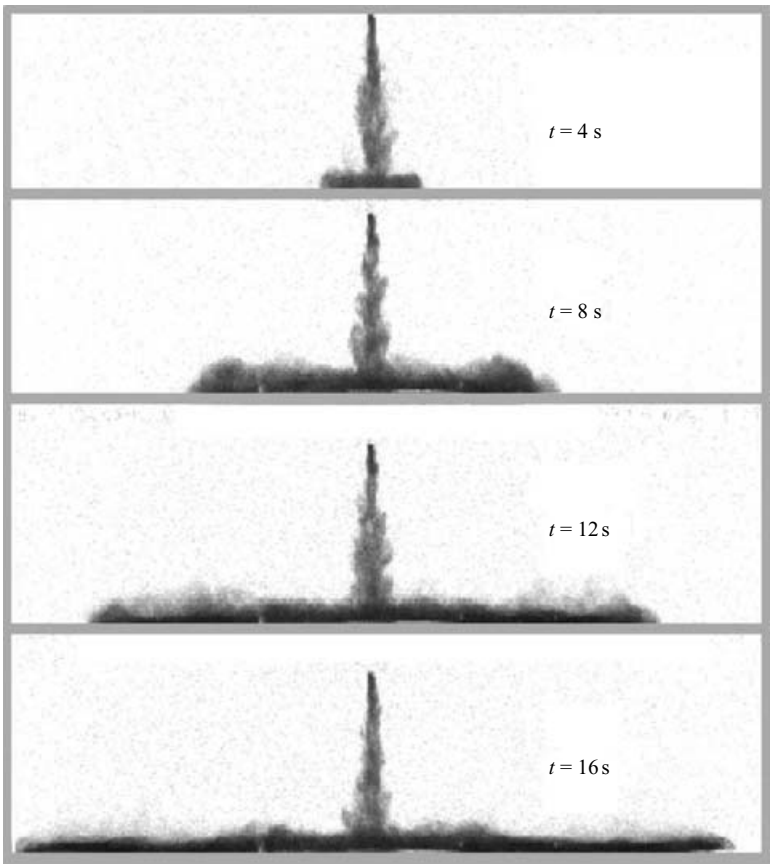

FIGURE 8. Series of digital images showing the descending plume and the horizontal outflow at various times during an experiment with $H = 8.5\,\text{cm}$ and $F = 255\,\text{cm}^4\,\text{s}^{-3}$.

measured. Owing to the different experimental configuration we were able to vary the source–boundary separation from 6.1 cm to 65.5 cm, which is considerably greater than the range achievable using our LIF setup. Using the scalings (2.26) we are able to collapse all the data from figure 9, and the additional 130 data points from the second series of experiments, on to a single line. These scaled front movement data are plotted in figure 10.

Based on the analysis presented in § 2 we expect that for small ϕ there would be a jet-like region where the front movement $\phi \sim \tau^{1/2}$ (2.27), followed by a pure gravity current region where $\phi \sim \tau^{3/4}$ (2.28). This behaviour is clearly seen in figure 10. The dashed line is given by $\phi = 0.85\tau^{1/2}$ and describes the near-source adjustment region, and the solid line is given by $\phi = 0.84\tau^{3/4}$, that is, (2.28), and describes well the fully adjusted constant Froude number flow. Our experimental agreement with the result of Britter (1979), along with (2.4) and (2.5), allows us to calculate the Froude number for the fully developed flow ($Fr \approx 1.49$). This is close to the value of $\sqrt{2}$, appropriate for large depth, constant buoyancy flux, parallel channel gravity currents (see Simpson 1982). However, we should note that this value for the Froude number is sensitive to the constant $C = 0.84$ from (2.28). The Froude number is given by $Fr = 3C^{4/3}\sqrt{2\pi}/4$.

We now compare the empirical relationship $\phi = 0.85\tau^{1/2}$ to (2.27). Firstly, we note that the power-law relationship (2.27) is the same as shown by the dashed line

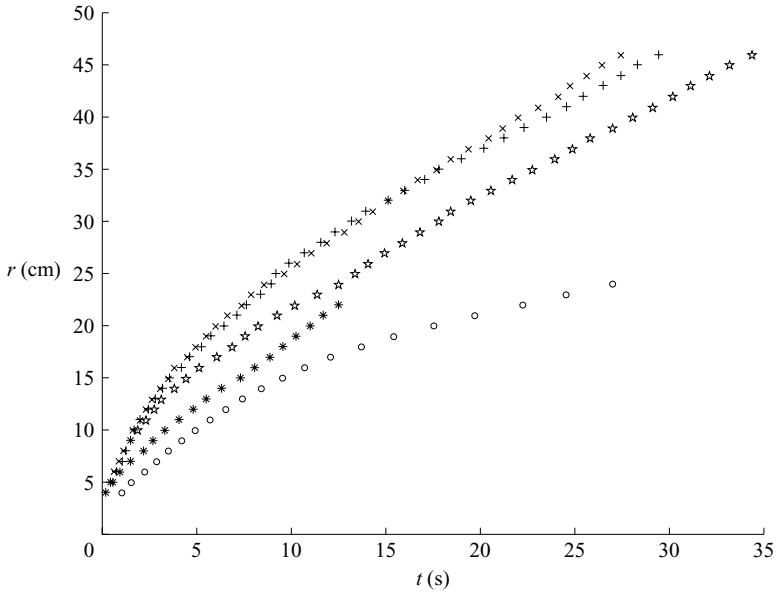

FIGURE 9. Plot of the front position r (cm) against time t (s) for experiments A to E. +, experiment A; ×, experiment B; ∗, experiment C; ⋆, experiment D; ○, experiment E.

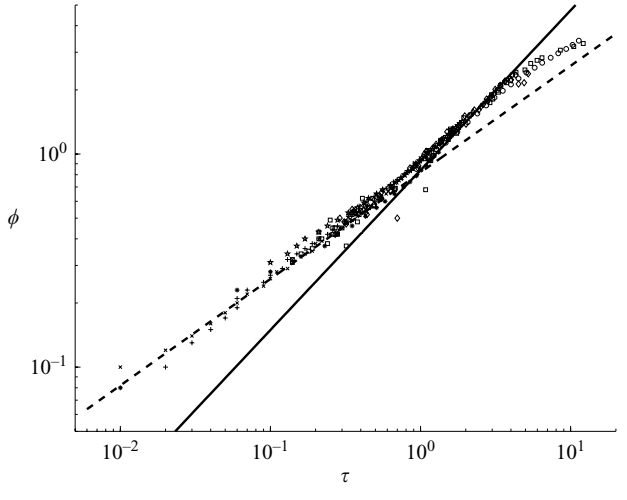

FIGURE 10. Non-dimensional outflow front position ϕ against time τ showing the collapse of the experimental data and the 'forced' jet-like region near the point of impingement, i.e. for small ϕ. The dashed line is given by $\phi = 0.85\tau^{1/2}$; cf. (2.27). The solid line is given by $\phi = 0.84\tau^{3/4}$; cf. (2.28). The discrepancy between the data and theory for large ϕ is due to the increasing influence of viscous forces.

in figure 10. The collapse of the data on to a single line implies that our scaling argument is valid and that the parameter γ can be considered a constant. It is also possible to do a numerical check on the estimate of $\gamma \approx 0.9$ suggested by Lee & Jirka (1981). In order to do this we need an estimate of $\mathrm{d}\Delta/\mathrm{d}r$. We approximate $\mathrm{d}\Delta/\mathrm{d}r \approx \Delta_a/r_a$, where $\Delta_a \approx 0.2H$ is the depth of the outflow at $r = r_a \approx 0.66H$. This leads to $\mathrm{d}\Delta/\mathrm{d}r \approx 0.3$. Substituting this value of $\mathrm{d}\Delta/\mathrm{d}r$ and $\gamma \approx 0.9$ into (2.27) leads

to $\phi = 0.91\tau^{1/2}$, which is very close to $\phi = 0.85\tau^{1/2}$ obtained from our experiments. Note that the front movement is not very sensitive to the value of γ. Performing the reverse calculation, and estimating γ based on (2.27) and our experimental result, leads to an estimate of $\gamma \approx 0.7$. Therefore, even if γ was not a constant, it actually has very little influence on the flow. Note also that both estimates are well above the value of $\gamma = 0.53$, below which the gravity current would not be forced at its source (2.20).

We have demonstrated that the outflow from a turbulent plume that impinges on a horizontal boundary behaves as a radial forced wall jet near the point of impingement and downstream as a pure radial gravity current. Our measurements demonstrate that the horizontal extent of the adjustment region scales linearly on the vertical separation H of the plume source from the horizontal boundary (figure 6). We have also demonstrated that the dimensionless front position $\phi = r/H$ can be described in terms of the non-dimensional time $\tau = t/(H^{4/3}F^{-1/3})$ by (2.27) and (2.28). Experimental results have shown that the full description of the front movement with time is given by:

$$\phi = \begin{cases} 0.85\tau^{1/2} & \text{for} \quad \phi < 0.66, \\ 0.84\tau^{3/4} & \text{for} \quad \phi \geqslant 0.66. \end{cases} \tag{5.2}$$

5.2. *Overturning experiments*

Given the uncertainty in the values of a number of parameters in our theoretical model, a series of experiments was conducted to establish these and the exact nature of the overturning motion in a cylindrical filling box. As with the measurements of the adjustment radius, a LIF technique was used, though the experiment was illuminated from the side rather than from below.

Two series of experiments were run. In series 1 the cylindrical tank was mounted on a bench, whereas in series 2 the tank was submerged in a larger rectangular glass tank to aid visualization. In both series the experimental procedure was the same. The plume nozzle was set to the desired height and the tank filled with fresh water. The water was then allowed to settle for approximately an hour so that there were no background disturbances. Once the tank had settled a constant volume flow rate of salt water, dyed with Sodium Fluorescein, was introduced through the nozzle. A light sheet projected from the side of the tank illuminated the plume flow as it descended, spread out at the tank base and rose as a fountain up the sidewall. At this point two flow modes were observed. For small aspect ratios (tall thin cylinders) the side-wall flow rolled back over toward the plume, engulfing ambient fluid below it. For larger aspect ratios the flow rose up the sidewall and would then slump back down without entraining additional ambient fluid but creating waves on the interface. A schematic of these two flow modes is shown in figure 11. Once the initial transient had passed the wall fountain was no longer discernible and the outflow was covered with a dense layer of fluid. The outflow model is then no longer valid as it does not account for any ambient stratification. This phase of the flow is beyond the scope of this work.

A series of images taken from two typical experiments are shown in figures 12 and 13. The plume outflow, rise up the sidewall and subsequent slumping or rolling back down can be clearly seen. Typically the slumping mode (figure 12), where the upflow collapses back down on itself, was observed for larger aspect ratios where the outflow is a fully developed gravity current when it reaches the sidewall. The rolling mode (figure 13), where the upflow rolls back over the outflow toward the plume centreline, was observed for smaller aspect ratios where the outflow is not fully developed and is still momentum-dominated.

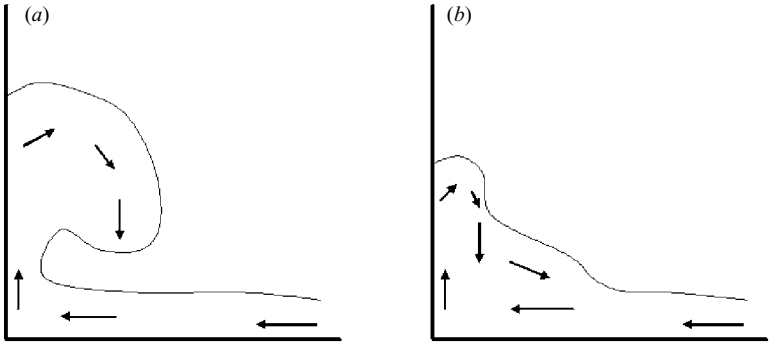

FIGURE 11. A schematic of the two overturning modes. (*a*) The rolling mode for tall thin cylinders that engulfs ambient fluid. (*b*) The slumping mode that does not engulf fluid but creates waves on the density interface.

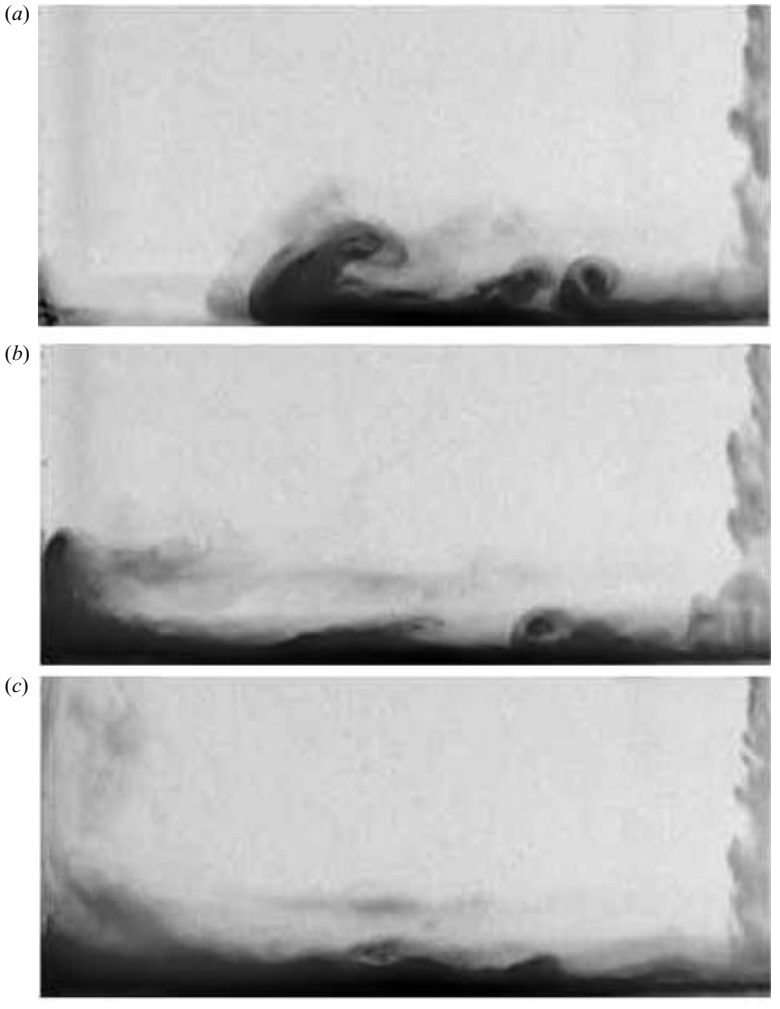

FIGURE 12. A series of three images, showing (*a*) the outflow from the plume, (*b*) the rise up the sidewall and (*c*) the slumping back. The right-hand boundary of each image is the plume centreline.

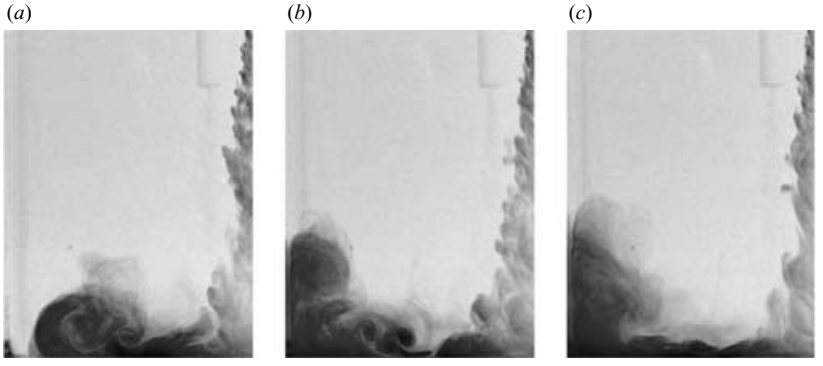

FIGURE 13. A series of three images showing (*a*) the outflow from the plume, (*b*) the rise up the sidewall and (*c*) the rolling back. The right-hand boundary of each image is the plume centreline.

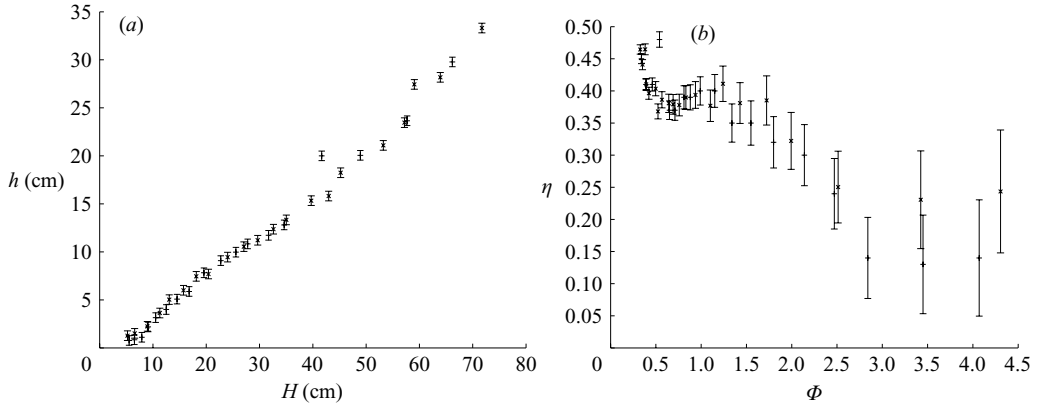

FIGURE 14. (*a*) Peak rise height up the sidewall h (cm) plotted against the source–boundary separation H (cm). Symbols represent the different experimental series, + series 1 and × series 2. (*b*) Dimensionless peak rise height η against the box aspect ratio Φ. Note that, as $\eta = h/H$, for smaller values of H the relative error in measuring η increases. As a result the difference between the h values for the five points where $\Phi > 2.5$ is only a matter of millimetres even though they appear much larger in this plot. The absolute difference is shown in figure 14(*a*).

The peak height up the sidewall prior to slumping or rolling was recorded. The raw data for the peak height (h) are plotted against source–boundary separation (H) in figure 14. The two experimental series are consistent and, within the accuracy of experimental measurements, collapse on to a single curve indicating that the problem is purely geometric. These raw results were then re-scaled to give the variables $\eta = h/H$ and $\Phi = R/H$ used in our model and are plotted next to the raw data in figure 14.

Over the range of Φ considered, there appears to be three separate regimes. For the larger aspect ratios considered ($\Phi > 1.5$) the rise height decreases with increasing aspect ratio. Typical experimental buoyancy fluxes were of the order of $180\,\mathrm{cm^4 s^{-3}}$, and taking H to be order $5-10\,\mathrm{cm}$ for these larger Φ experiments leads to a Reynolds number based on (4.17) of $Re = 1300 - 2600$. Substituting these values into (4.18), we get $\Phi_* \approx 1.5 - 2$. This would tend to indicate that, in our experiments, for $\Phi \gtrsim 1.5$ the outflow will be influenced by viscosity. For small aspect ratios the peak rise height

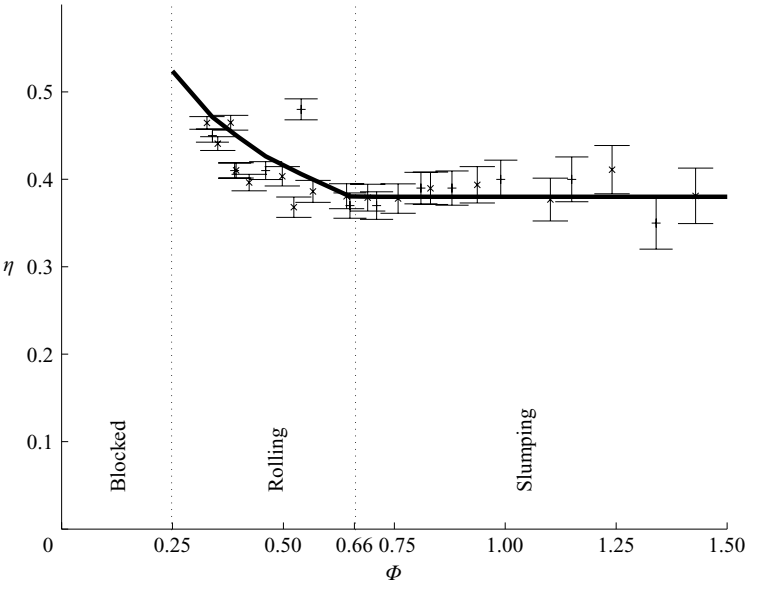

FIGURE 15. Dimensionless peak rise height η as a function of the cylinder aspect ratio Φ for the range $\Phi < 1.5$ showing the fit (5.3). The dashed lines mark the boundaries between the blocked, rolling, and slumping modes.

η appears to grow inversely proportional to the aspect ratio. This is expected based on (4.14). Although it is not clear what the exact relationship is, (4.13) appears to be applicable for $\Phi \lesssim 0.6$. Between these two regions there is significant scatter. However, whatever functional form the data follow, it appears to be only a very weak function of the aspect ratio.

We now attempt to match our scaling results of (4.14) to our experimental results. Assuming that the constant rise height regime occurs for $0.66 < \Phi < 1.5$, we take the average of all points in this region and get a value of $\eta_{avg} = 0.38$. Assuming that the function $\eta(\Phi)$ is continuous at $\Phi = 0.66$, we then substitute $\eta = 0.38$ into both parts of (4.14) to get

$$\left.\begin{array}{lll} \eta \approx 0.33\Phi^{-1/3} & \text{for} & \Phi < 0.66, \\ \eta \approx 0.38 & \text{for} & \Phi \geqslant 0.66. \end{array}\right\} \tag{5.3}$$

In order to verify the applicability of this result for $\Phi < 0.66$ we have re-plotted our experimental data for $0.25 < \Phi < 1.5$ along with (5.3) in figure 15. There is good agreement between our experimental data and the scaled theoretical predictions, indicating that the $-1/3$ third power-law scaling is appropriate for estimating the rise height up the sidewall of the plume outflow in an axisymmetric filling box. The full expression for the rise height is therefore

$$\left.\begin{array}{lll} \text{Plume blocked} & & \text{for} \quad \Phi < 0.25, \\ \text{Rolling} & \eta \approx 0.33\Phi^{-1/3} & \text{for} \quad 0.25 < \Phi < 0.66, \ \Phi < 0.1Re^{3/8}, \\ \text{Slumping} & \eta \approx 0.38 & \text{for} \quad \Phi \geqslant 0.66, \ \Phi < 0.1Re^{3/8}. \end{array}\right\} \tag{5.4}$$

6. Conclusions

We have developed a model for the overturning of the flow driven by a plume in a closed cylindrical box, namely, an axisymmetric filling box. The model was developed

by separating the flow into three distinct regions, the plume flow, the outflow due to impingement on the box base, and the flow rising up the sidewall. The plume was modelled as a pure plume using the results of Morton *et al.* (1956). The outflow was modelled as a constant-flux forced radial turbulent gravity current (see § 2) and the flow up the sidewall was treated as a turbulent line fountain (see § 3).

Based on these results we were able to establish that the rise height as a function of the box aspect ratio fell into two regimes. First, when the outflow was fully adjusted to a pure gravity current, the rise height scaled on the box height, and was independent of the radius (4.8). Secondly, when the outflow hit the sidewall while in the forced adjustment region, the rise height scaled on the aspect ratio to the power of minus one third (4.13). These relationships were assumed to hold provided that the viscous forces are negligible (4.18) and the box was wide enough (4.19).

Experiments were conducted to verify that the scaling relationships of (4.14) were appropriate, and to establish the constants required to complete the model. Experiments over a wide range of aspect ratios showed good qualitative agreement with the model proposed, and allowed a full expression for the rise height as a function of aspect ratio to be established (5.4).

The authors gratefully acknowledge the financial support of BP through their Advanced Energy in Buildings Programme at Imperial College London.

REFERENCES

Alpert, R. L. 1975 Turbulent ceiling jet induced by large-scale fires. *Combust. Sci. Tech.* **11**, 197–213.

Baines, W. D. & Turner, J. S. 1969 Turbulent buoyant convection from a source in a confined region. *J. Fluid Mech.* **37**, 51–80.

Baines, W. D., Turner, J. S. & Campbell, I. H. 1990 Turbulent fountains in an open chamber. *J. Fluid Mech.* **212**, 557–592.

Bakke, P. 1957 An experimental investigation of a wall jet. *J. Fluid Mech.* **2**, 467–472.

Barnett, S. J. 1991 The dynamics of buoyant releases in confined spaces. PhD thesis, DAMTP, University of Cambridge.

Britter, R. E. 1979 The spread of a negatively buoyant plume in a calm environment. *Atmos. Environ.* **13**, 1241–1247.

Chen, J. C. & List, E. J. 1977 Spreading of buoyant discharges. In *Proc. 1976 ICHMT Seminar on Turbulent Buoyant Convection*, pp. 171–182.

Cooper, L. Y. 1988 Ceiling jet-driven wall flows in compartment fires. *Combust. Sci. Tech.* **62**, 285–296.

Dalziel, S. B. 1993 Rayleigh–Taylor instability: experiments with image analysis. *Dyn. Atmos. Oceans* **20**, 127–153.

Goldman, D. & Jaluria, Y. 1986 Effect of opposing buoyancy on the flow in free and wall jets. *J. Fluid Mech.* **166**, 41–56.

Hacker, J., Linden, P. F. & Dalziel, S. B. 1996 Mixing in lock-release gravity currents. *Dyn. Atmos. Oceans* **24**, 183–195.

Hunt, G. R., Cooper, P. & Linden, P. F. 2001 Thermal stratification produced by plumes and jets in enclosed spaces. *Building Environ.* **36**, 871–882.

Hunt, G. R. & Kaye, N. G. 2001 Virtual origin correction for lazy turbulent plumes. *J. Fluid Mech.* **435**, 377–396.

Hunt, G. R. & Kaye, N. B. 2005 Lazy plumes. *J. Fluid Mech.* **533**, 329–338.

Hunt, G. R. & Kaye, N. B. 2006 Pollutant flushing with natural displacement ventilation. *Building Environ.* **41**, 1190–1197.

Huppert, H. E., Sparks, R. S. J., Whitehead, J. A. & Hallworth, M. A. 1986 Replenishment of magma chambers by light inputs. *J. Geophys. Res.* **91**, 6113–6122.

Jaluria, Y. & Kapoor, K. 1992 Wall and corner flows driven by a ceiling jet in an enclosure fire. *Combust. Sci. Tech.* **18**, 311–326.

Kapoor, K. & Jaluria, Y. 1996 Flow and heat transfer due to a buoyant ceiling jet turning downward at a corner. *Trans. ASME: J. Heat Transfer* **118**, 38–46.

Kaye, N. B. & Hunt, G. R. 2006 Weak fountains. *J. Fluid Mech.* **558**, 319–328.

Lawrence, G. A. & MacLatchy, M. R. 2001 Radially spreading buoyant flows. *J. Hydraul. Res.* **39**, 583–590.

Lee, J. H. W. & Jirka, G. H. 1981 Vertical round buoyant jet in shallow water. *J. Hydraul. Div. Proc. ASCE* **107**, 1651–1975.

Linden, P. F., Lane-Serff, G. F. & Smeed, D. A. 1990 Emptying filling boxes, the fluid mechanics of natural ventilation. *J. Fluid Mech.* **212**, 309–335.

Manins, P. C. 1979 Turbulent buoyant convection from a source in a confined region. *J. Fluid Mech.* **91**, 765–781.

Morton, B. R. 1959 Forced plumes. *J. Fluid Mech.* **5**, 151–163.

Morton, B. R., Taylor, G. I. & Turner, J. S. 1956 Turbulent gravitational convection from maintained and instantaneous sources. *Proc. R. Soc. Lond.* A **234**, 1–23.

Patterson, M. D., Simpson, J. E., Dalziel, S. B. & van Heijst, G. J. F. 2006 Vortical motion in the head of an axisymmetric gravity current. *Phys. Fluids* **18**, 046601–1–7.

Simpson, J. E. 1982 Gravity currents in the laboratory, atmosphere, and ocean. *Annu. Rev. Fluid Mech.* **14**, 213–234.

Turner, J. S. 1962 The 'starting plume' in neutral surroundings. *J. Fluid Mech.* **13**, 356–368.

Turner, J. S. 1966 Jets and plumes with negative or reversing buoyancy. *J. Fluid Mech.* **26**, 779–792.

Wilkinson, D. L. & Wood, I. R. 1971 A rapidly varied flow phenomenon in a two-layer flow. *J. Fluid Mech.* **47**, 241–256.

Wong, A. B. D., Griffiths, R. W & Hughes, G. O. 2001 Shear layers driven by turbulent plumes. *J. Fluid Mech.* **434**, 209–241.

Worster, M. G. & Huppert, H. E. 1983 Time-dependent density profiles in a filling box. *J. Fluid Mech.* **132**, 457–466.